

1  
2  
3  
4  
5  
6  
7  
8  
9  
10  
11  
12  
13  
14  
15  
16  
17  
18  
19  
20  
21  
22  
23  
24  
25  
26

**A SYNOPTIC-CLIMATOLOGY OF NORTHERN HEMISPHERE, COLD SEASON  
POLAR AND SUBTROPICAL JET SUPERPOSITION EVENTS**

*by*

CROIX E. CHRISTENSON, JONATHAN E. MARTIN  
and ZACHARY J. HANDLOS

*Department of Atmospheric and Oceanic Sciences  
University of Wisconsin-Madison  
1225 W. Dayton Street  
Madison, WI 53705  
[jemarti1@wisc.edu](mailto:jemarti1@wisc.edu)*

Submitted for publication in *XXXXXX*:  
August 2016

27  
28  
29  
30  
31  
32  
33  
34  
35  
36  
37  
38  
39  
40  
41  
42  
43  
44  
45  
46

## ABSTRACT

Narrow, tropopause-level wind speed maxima known as jet streams or jets are among the most ubiquitous structural characteristics of the Earth’s atmosphere. Two jet species can be observed on any given day. The polar jet is tied, via eddy momentum flux convergence associated with extratropical wave development, to the troposphere-deep baroclinicity of the middle latitudes while the subtropical jet is tied, by angular momentum constraints, to the poleward edge of the tropical Hadley Cell. As a consequence of their different origins, the polar and subtropical jets are separated by both latitude and elevation. However, there are times when these two usually separate features become vertically superposed to form a single, intense jet core designated as a jet superposition or superposed jet.

An objective method for identifying tropopause-level jets is employed in the construction of 50-year cold season (NDJFM) synoptic-climatologies of the Northern Hemisphere polar jet, subtropical jet, and jet superpositions. The analysis demonstrates that while superposition events are relatively rare, there are clear geographical maxima. Superpositions are most frequent in the western Pacific from December through February, with a secondary peak in southern North America and along its eastern seaboard. Consistent with expectations, the spatiotemporal maxima in jet superpositions appear to be coincident with maxima in the polar and subtropical jets.

46

47 **1. Introduction**

48           Narrow, rapidly flowing currents of air located near the tropopause are known as jet  
49 streams or jets. These jets, often found nearly girdling the globe while exhibiting large  
50 meridional meanders, are among the most ubiquitous structural characteristics of the Earth's  
51 atmosphere and are known to play a substantial role in the production of sensible weather in the  
52 mid-latitudes. Prior observational work has identified three major jet features; the subtropical  
53 jet, the polar jet, and the Arctic jet.

54           The subtropical jet is located at the poleward edge of the Hadley cell ( $\sim 30^\circ$  latitude) in  
55 the tropical/subtropical upper troposphere ( $\sim 200$  hPa) (Loewe and Radok 1950, Yeh 1950,  
56 Koteswaram 1953, Mohri 1953, Koteswarma and Parthasarathy 1954; Sutcliffe and Bannon  
57 1954, Defant and Taba 1957, Krishnamurti 1961, Riehl 1962) and is driven by angular  
58 momentum transport forced by low latitude convection. The polar jet sits atop the baroclinicity  
59 of the middle latitudes (usually poleward of  $30^\circ$  latitude) and has its speed maxima closer to 300  
60 hPa (e.g. Namias and Clapp 1949, Newton 1954, Palmén and Newton 1969, Keyser and Shapiro  
61 1986, Shapiro and Keyser 1990).

62           Namias and Clapp (1949) first discussed the polar jet from the perspective of confluence,  
63 which drives horizontal frontogenesis. The subsequent concept of the eddy-driven jet is an  
64 elaboration of this original insight, suggesting that the polar jet results from the convergence of  
65 eddy momentum flux associated with developing waves in a region of enhanced mid-latitude  
66 baroclinicity (Held 1975, Rhines 1975, McWilliams and Chow 1981, Panetta 1993). Though  
67 often identified by a lower tropospheric westerly wind maximum (Lorenz and Hartmann 2003),  
68 the polar jet is associated with its own tropopause undulation as can be discerned by routine

69 inspection of vertical cross-sections of wind speed and potential vorticity (PV). The arctic jet is  
70 less ubiquitous but is confined to high latitudes and is often located at ~500 hPa (Shapiro et al.  
71 1984, Shapiro 1985, Shapiro et al. 1987).

72 Careful observational work by Defant and Taba (1957, hereafter DT57) established the  
73 existence of a three step structure in tropopause height from pole-to-equator with each step  
74 separated from its neighbors by the presence of a westerly wind maximum. The tropical  
75 tropopause was found (in the mean) to be at ~90 hPa (17 to 18 km) and to extend to about 30°N.  
76 Near that latitude, the tropopause height abruptly lowers to ~200 hPa. The subtropical jet is  
77 coincident with this break in tropopause height and is located at ~200 hPa (12 km). Poleward of  
78 this feature was what DT57 called the “middle tropopause” located at ~250 hPa. At the break  
79 between this middle tropopause and the even lower polar tropopause is the polar jet, located at  
80 ~300 hPa. Modest, shallow baroclinicity in the upper troposphere characterizes the subtropical  
81 jet whereas the much deeper and more dramatically baroclinic polar front drapes below the polar  
82 jet.

83 A new insight represented by the DT57 analysis was their construction of maps of  
84 tropopause height (in hPa). They referred to sharp, isolated, easily identifiable gradients of  
85 tropopause height as “breaklines” (see their Fig. 2). These breaklines were found to be  
86 coincident with the axes of the respective jet maxima (e.g. the subtropical jet was located at the  
87 breakline between the tropical and middle tropopause)<sup>1</sup>. Such depictions made it instantly clear  
88 that, though each jet maximum occupied a climatological latitude band, substantial meanders of  
89 each were commonplace. Companion maps of tropopause temperature presented by DT57  
90 clearly demonstrated that when the polar and subtropical jets become latitudinally superposed the

---

<sup>1</sup> Equation 1 (to be discussed later) demonstrates that local maxima in the geostrophic wind,  $V_g$ , are coincident with large horizontal gradients of quasi-geostrophic potential vorticity (QGPV).

91 tropospheric and stratospheric baroclinicity associated with each jet individually were combined  
92 into substantially narrower zones of contrast. The resulting superposed jet structure therefore  
93 possessed an anomalous fraction of the pole-to-equator baroclinicity (manifest as available  
94 potential energy (APE)).

95 An alternative method for identifying the tropopause breaklines of DT57 lies in the  
96 construction of tropopause maps in potential temperature/potential vorticity ( $\theta$ /PV) space. Such  
97 an approach was advocated by Morgan and Nielsen-Gammon (1998) who demonstrated the  
98 utility of maps of  $\theta$  and wind speed on the so-called dynamic tropopause (defined as a surface of  
99 constant Ertel PV (Ertel 1942)) for diagnosing weather systems. In this framework, the DT57  
100 breaklines become regions of large PV gradient on isentropes that cut through the subtropical  
101 and polar jet cores since such isentropes sample both stratospheric and tropospheric air.

102 By virtue of their enhanced wind speeds and baroclinicity, superposed jets are  
103 characterized by invigorated horizontal and vertical circulations (Handlos and Martin 2016) and  
104 have been connected, either directly or indirectly, with a number of previously examined high  
105 impact, mid-latitude sensible weather phenomena. Defant (1959) noted that an exceptional  
106 surface cyclogenesis event south of Iceland on 8 January 1956, in which the sea-level pressure  
107 (SLP) dropped 61 hPa in 20 h, developed in an environment characterized by a dramatic jet  
108 superposition event. Other famous explosive cyclogenesis events such as the Great October  
109 Storm (Hoskins and Berrisford 1988), the ERICA IOP-4 storm (Shapiro and Keyser 1990), the  
110 Cleveland Superbomb (Hakim et al. 1996), and the Storm of the Century (Bosart et al. 1996) are  
111 all examples of developments likely influenced by a jet superposition event<sup>2</sup>.

---

<sup>2</sup> At some point in their respective evolutions, all of these cases were characterized by a two-step tropopause structure similar to that portrayed in Fig. 1d.

112 More recently, Winters and Martin (2014, 2016a) examined the influence the secondary  
113 circulations associated with superposed jet structures had in forcing a rapid increase in poleward  
114 moisture flux that fueled the second day of the 2010 Nashville Flood and in the development of a  
115 major winter storm in the northeastern United States. In addition, the 25-28 April 2011 severe  
116 weather outbreak across the central and eastern portion of North America (Christenson and  
117 Martin 2012 and Knupp et al. 2014) has been linked to a superposed jet structure that formed  
118 over the west Pacific Ocean.

119 Superposition events also exhibit ties to elements of the Northern Hemisphere large-scale  
120 circulation. In their examination of the large-scale environments conducive to jet superposition  
121 in the west Pacific, Handlos and Martin (2016) showed that these events are by-products of the  
122 surge phase of the East Asian Winter Monsoon (EAWM). Additionally, Handlos (2016) has  
123 shown that such events lead to zonal extension of the jet, a leading mode of Pacific jet variability  
124 (Eichelberger and Hartmann 2007, Athanasaidis et al. 2010, Jaffe et al. 2011, Griffin and Martin  
125 2016).

126 Despite the appearance of jet superposition events as a fundamental ingredient in a  
127 number of high impact, mid-latitude weather environments, and their association with large-scale  
128 circulation phenomena during the cold season (November – March, hereafter NDJFM) there is  
129 no synoptic-climatology of these features nor any systematic observational study of the  
130 mechanism(s) by which the polar and subtropical jets become vertically superposed. It is the goal  
131 of this paper to provide a cold season synoptic-climatology of Northern Hemisphere jet  
132 superpositions.

133 The paper is organized as follows. Section 2 provides a description of the data sets and  
134 methodology used to objectively identify the polar jet, subtropical jet, and locations where the

135 two are vertically superposed. Section 3 presents the results of a 50-year, cold season synoptic-  
 136 climatology of the frequency and distribution of each species of tropopause-level jet. The  
 137 climatology of jet superposition events is presented in Section 4. Finally, Section 5 discusses the  
 138 results in the context of other studies of jet stream climatology and offers final comments and  
 139 conclusions, along with suggestions for future work.

140

## 141 **2. Data and methodology**

142

143 Considered from a PV perspective, the subtropical and polar jets are each associated with  
 144 local positive PV perturbations at the equatorward edge of the tropopause. Most often, the  
 145 separate jet cores, as well as the separate PV perturbations, are readily identifiable as illustrated  
 146 in Figs. 1a&b. Note that the PV distribution displayed in Fig. 1b portrays the 3-step tropopause  
 147 structure identified by DT57. Note also that the separate polar and subtropical jet cores, though  
 148 widely separated in latitude and elevation, are each found at a “break” in dynamic tropopause  
 149 height represented by a locally steep tropopause slope. A superposed jet structure cannot be  
 150 identified solely by inspection of the distribution of isotachs on an isobaric surface (Fig. 1c).  
 151 Instead, the distinguishing structural characteristic of such features is the vertical tropopause wall  
 152 directly connecting the tropical tropopause to the polar tropopause (Fig. 1d). The development  
 153 of such a structure has dynamical implications that are most simply considered from the quasi-  
 154 geostrophic PV (QGPV) perspective. Recalling that QGPV is given by

155

$$q_g = \frac{1}{f_o} \nabla^2 \phi + f + \frac{\partial}{\partial p} \left( \frac{f_o}{\sigma} \frac{\partial \phi}{\partial p} \right) = \Lambda(\phi) + f$$

156

(where  $\Lambda = \frac{1}{f_o} \nabla^2 + \frac{\partial}{\partial p} \left( \frac{f_o}{\sigma} \right) \frac{\partial}{\partial p} + \frac{f_o}{\sigma} \frac{\partial^2}{\partial p^2}$ ). The cross-jet gradient of QGPV is then given by

157 
$$\frac{\partial q_g}{\partial n} = \Lambda\left(\frac{\partial \phi}{\partial n}\right) = \Lambda(-fV_g) \quad (1)$$

158 after substituting from the natural coordinate expression for the geostrophic wind (Cunningham  
 159 and Keyser 2004). The deep tropopause wall arises via an increase in  $\frac{\partial q_g}{\partial n}$  through a deep layer  
 160 (i.e.  $-\frac{\partial}{\partial p}\left[\frac{\partial}{\partial t}\left(\frac{\partial q_g}{\partial n}\right)\right] > 0$ ). It follows from (1) that in such an environment

161 
$$f\Lambda\left[\frac{\partial}{\partial t}\left(\frac{\partial V_g}{\partial p}\right)\right] > 0.$$

162 Since  $\Lambda$  is a Laplacian operator, this implies that the development of a deep tropopause wall  
 163 requires a local increase in the (geostrophic) vertical shear (i.e.  $\frac{\partial}{\partial t}\left(-\frac{\partial V_g}{\partial p}\right) > 0$ ). Thus, it is  
 164 hypothesized that superposition of the polar and subtropical jets can bring about rapid and  
 165 substantial increases in jet speeds as well as strengthening of the associated divergent  
 166 ageostrophic circulations.

167 A central analysis question thus becomes which isentropic layers most frequently house  
 168 the separate polar and subtropical jets? Various prior studies (e.g. Defant and Taba 1957,  
 169 Palmén and Newton 1969, Shapiro et al. 1987, Morgan and Nielsen-Gammon 1998, Mecikalski  
 170 and Tripoli 1998, Shapiro et al. 1999, and Randel et al. 2007) have suggested a fairly narrow  
 171 range of acceptable values; 310–320K for the polar jet and 335-345K for the subtropical jet. In  
 172 the present work, the choice is made via two rather distinct analyses of 50 years of NCEP  
 173 Reanalysis data (1960-61 to 2009-10).

174 The first method begins by interpolating the data into 5K isentropic layers spanning from  
 175 300-305K to 375-380K. The interpolated data are then employed to calculate PV in each layer.  
 176 Since the jets are tied to the low-PV edge of the strong PV gradient at the tropopause, the



177 magnitude of the zonally averaged PV gradient between the 1 and 3 PVU isertels in each layer  
 178 for each day is calculated in the following manner. In each layer, the area ( $A$ ) enclosed by the 1  
 179 PVU isertel is calculated and then converted to an equivalent latitude by the formula

$$180 \quad \phi_e = a \sin \left[ 1 - \frac{A}{2\pi R_e^2} \right]$$

181 where  $R_e$  is the radius of the earth. After applying the same procedure to the 3 PVU isertel, the  
 182 meridional distance between the two equivalent latitudes,  $\Delta y$ , is an inverse measure of the  
 183 intensity of the zonally averaged 1-3 PVU gradient in that layer on that day. Daily averages of  
 184  $\Delta y$  in each layer over the 50 seasons are calculated next. To further smooth the data, we  
 185 calculate the cold season average of these daily average values. The resulting November 1 –  
 186 March 31 average  $\Delta y$  in each layer is plotted in Fig. 2a. The analysis reveals two minima in  $\Delta y$   
 187 (maxima in  $|\nabla PV|$ ) and that they occupy the 315-330K and 340-355K isentropic layers.

188 In support of the foregoing analysis, we also considered the isentropic level at which the  
 189 maximum wind speed was observed in each grid column (between 10-80°N) at each analysis  
 190 time in the 50-year time series. Note that only grid columns in which the maximum wind speed  
 191 exceeded  $30 \text{ ms}^{-1}$  within the 100-400 hPa layer were considered in the census. The results of this  
 192 analysis indicate a clear bi-modal distribution with twin frequency maxima in the 310-325 and  
 193 340-355K layers (Fig. 2b). The combined analyses in Fig. 2 compel adoption of the 315-330 and  
 194 340-355K layers as the respective isentropic space residences of the polar and subtropical jets.

195 The climatology is constructed from 50 cold seasons (NDJFM) of National Center for  
 196 Environmental Prediction – National Center for Atmospheric Research (NCEP-NCAR)  
 197 reanalysis data, at 6 hour intervals, spanning the period 1 November 1960 to 31 March 2010. The  
 198 NCEP-NCAR reanalysis data are available at 17 isobaric levels (1000, 925, 850, 700, 600, 500,  
 199 400, 300, 250, 200, 150, 100, 70, 50, 30, 20, and 10 hPa) with a  $2.5^\circ$  latitude-longitude grid

200 spacing (Kalnay et al. 1996, Kistler et al. 2001). These data were bi-linearly interpolated onto  
201 isentropic surfaces at 5K intervals from 300K to 370K using programs within the General  
202 Meteorology Package (GEMPAK) (desJardins et al. 1991).

203 In order to identify the polar, subtropical and superposed jet streams an automated,  
204 objective identification scheme was developed whose criteria can be described with reference to  
205 the features illustrated in Fig. 1 and the analysis described in the prior section. Figure 1a clearly  
206 portrays two distinct jets located off the west coast of North America with the polar jet feature  
207 near the Oregon, Washington border and the subtropical jet zonally oriented over Mexico. A  
208 vertical cross section taken through the polar and subtropical jet cores (Fig. 1b) shows that the  
209 polar jet, located at approximately 300 hPa, is largely contained within the 315-330K isentropic  
210 layer while the subtropical jet core, located at approximately 200 hPa, occupies the 340-355K  
211 layer. Additionally, both the polar and the subtropical jets lie at the low PV edge of the strong  
212 horizontal PV gradient that separates the upper troposphere from the lower stratosphere within  
213 each respective isentropic layer. The PV isertels are locally quite steep in the vicinity of the jet  
214 cores. In fact, considering the 2 PVU contour as the dynamic tropopause, it is clear that the  
215 tropopause breaklines of DT57, which portrayed the steep slope of the tropopause near the jet  
216 axes, are exactly equivalent to regions of large  $|\nabla_n PV|$  in the 1-3 PVU channel, which represents  
217 the boundary between the stratosphere and troposphere. Given these basic structural elements,  
218 the identification scheme evaluates characteristics of the PV and wind speed distributions in each  
219 grid column. Within the 315-330K (340-355K) layer, whenever the magnitude of the PV  
220 gradient within the 1-3 PVU channel exceeds an empirically determined threshold value<sup>3</sup> and the

---

<sup>3</sup> The threshold value is  $0.64 \times 10^{-5}$  PVU  $m^{-1}$  ( $0.64 \times 10^{-11}$  m K  $kg^{-1}$   $s^{-1}$ ) for both the 315-330K and 340-350K layers. This value was determined by extensive analysis of vertical cross-sections through jets in order to determine the minimum value of  $|\nabla_n PV|$  required to reliably identify the deep tropopause wall characteristic of superposed jets. For

221 integrated wind speed in the 400-100 hPa layer exceeds  $30 \text{ m s}^{-1}$ , we identify a polar  
222 (subtropical) jet in that grid column.

223 Occasionally, the two jets superpose in the vertical, creating a hybrid of both the subtropical  
224 and polar jets, as illustrated in Fig. 1c. A vertical cross-section taken through the jet core, as  
225 shown in Fig. 1d, thus illustrates that the criteria for both the polar and subtropical jet are  
226 identified in a single vertical grid column, identifying a superposed jet. Notice that, rather than  
227 the three-step tropopause structure identified by DT57 and shown in Fig. 1b, a superposed jet is  
228 characterized by a two-step tropopause structure with a steep tropopause break from the polar to  
229 the tropical tropopause. This nearly vertical PV wall (from  $\sim 550 \text{ hPa}$  to  $\sim 150 \text{ hPa}$  in this case) is  
230 a leading structural characteristic of these features.

231 The identification scheme is applied to each 6 h analysis time in the 50 cold seasons to  
232 objectively identify grid point locations of the subtropical jet, polar jet and jet superposition  
233 events<sup>4</sup>. The identifications are then compiled to reveal the spatial and temporal distribution of  
234 all three tropopause-level jet species. In addition, the speed and direction of the wind at 250hPa  
235 is recorded for each grid column in which a jet superposition is identified.

236

### 237 **3. Analysis of jet distributions**

238

239 In this section the results of the objective identification of the polar and subtropical jet  
240 species are presented as frequency distributions in both seasonal and monthly form. The analysis  
241 begins by considering the frequency distributions for the polar jet.

---

each isentropic layer, the threshold value exceeds the 50<sup>th</sup> percentile for  $|\nabla_n PV|$  in grid columns located in the 1-3 PVU channel with integrated wind speed exceeding  $30 \text{ m s}^{-1}$ .

<sup>4</sup> The total number of possible identifications for each grid point in each month of a given year is equal to the number of days in the month x 4. (Example: For a given grid point, each January, with 31 days in the month, would have 124 possible identifications.)

242  
243  
244  
245  
246  
247  
248  
249  
250  
251  
252  
253  
254  
255  
256  
257  
258  
259  
260  
261  
262  
263  
264  
265

*a. Polar Jet*

During the Northern Hemisphere cold season (NDJFM), the polar jet is found most frequently over the eastern portions of North America and the northern portions of the Atlantic Ocean (Fig. 3a). In the Pacific basin the polar jet is distributed rather uniformly with localized maxima located south of Alaska and near Japan. Notably, the polar jet is far less frequent over the eastern hemisphere than over the western hemisphere. Partitioning the cold season into its constituent months reveals a number of interesting subseasonal characteristics in the frequency and distribution of the polar jet.

The November frequency distribution (Fig. 4a) is characterized by separate maxima near Japan and south of Alaska. The axis of maximum polar jet frequency over the Atlantic sector stretches from central North America to the British Isles. In December narrow latitude bands of maximum frequency exist in the western portions of both ocean basins (Fig. 4b). These bands broaden across the basin from west to east indicating greater variability of the flow in the eastern portions of both basins. Also worthy of note is the fact that the axis of greatest frequency in both basins shifts dramatically equatorward from November to December.

January has a similar frequency distribution as December with a continued but less dramatic shift equatorward in both basins (Fig. 4c). Interestingly, the polar jet remains much more common in the Atlantic than in the Pacific basin although the west Pacific basin frequency maxima continues to narrow and extend zonally. By February, the Atlantic (Pacific) frequency maxima has decreased (increased) slightly with the only other notable change being a decrease in polar jet frequency extending from the west coast of North America to the south central Plains of the United States (Fig. 4d).

266 A dramatic shift in the hemispheric frequency maxima from the Atlantic to the Pacific  
267 (Fig. 4e) characterizes the distribution in March. The frequency maxima in the Pacific (Atlantic)  
268 basin also increases (decreases) during March. While barely noticeable in Fig. 4e, the polar jet  
269 shifts  $2.5^{\circ}$  northward during March in the western Pacific basin as it begins its poleward  
270 migration north for the summer.

271

### 272 *b. Subtropical Jet*

273

274 During the Northern Hemisphere cold season the subtropical jet has a frequency maxima  
275 in the western Pacific, over Japan, that extends westward to southern China and eastward to the  
276 dateline (Fig. 3b). This local maxima is embedded within an axis of maximum frequency that  
277 stretches across the entire eastern hemisphere at  $\sim 30^{\circ}\text{N}$ . The central Pacific and southern North  
278 America, along with northwest Africa, are other regions with frequent subtropical jet activity  
279 during the cold season.

280 In November the subtropical jet frequency maxima in the Pacific, previously spread over  
281 a wide latitude band in the western Pacific basin (not shown) is consolidated into a narrow  
282 latitudinal strip centered on Japan (Fig. 5a). The wide band of low frequency distribution over  
283 North America and the north Atlantic testifies to the variability of the subtropical jet location in  
284 these regions during November. By December, the axis of maximum subtropical jet frequency  
285 has expanded both eastward and westward but remains fixed near  $32.5^{\circ}\text{N}$  while the maximum in  
286 frequency has increased to greater than 25 times per month in some locations (Fig. 5b). January  
287 represents the month of maximum subtropical jet frequency with a large swath of greater than 31  
288 identifications per month along the north coast of Japan (Fig. 5c). January is also the first month  
289 that exhibits a thin band of greater than 7 identifications per month stretching westward from the

290 southern portion of Asia to North Africa. February has nearly the same hemispheric distribution  
291 as January but with a small reduction in the west Pacific frequency maxima (Fig. 5d).  
292 Throughout the winter months, the subtropical jet frequency maxima shifts westward (Figs. 5b-  
293 d). The distribution in March is quite similar to the distributions in the preceding winter months  
294 albeit with reduced frequencies (Fig. 5e).

295

#### 296 **4. Jet superpositions**

297

298 As described previously, a jet superposition (alternatively, a *superposed jet*) occurs when  
299 both the polar jet and subtropical jet are identified in the same vertical grid column. In this  
300 section the frequency distribution of such structures is presented.

301

##### 302 *a. Distribution of jet superpositions*

303

304 The cold season distribution of jet superpositions is clearly maximized in the west Pacific  
305 basin just east of Japan (Fig. 3c). A secondary frequency maxima stretches across southern  
306 North America out to the southern Maritime Provinces of Canada. The third very weak local  
307 frequency maxima is evident over the southeastern Mediterranean Sea. Monthly frequency  
308 distributions, again, provide a refined perspective on the characteristic cold season circulation  
309 evolution.

310 November superposition events occur across the entire Pacific basin with a slight  
311 frequency maximum east of Japan (Fig. 6a). A separate axis of frequency maximum stretches  
312 from the central United States toward the north Atlantic (Fig. 6a). By December, the robust local

313 maximum in jet superposition events in the western Pacific first presents itself (Fig. 6b). This  
314 dramatic increase results from an increased frequency, as well as a decreased variability, of both  
315 the subtropical and polar jets in this region at this time of year. In fact, in December the axis of  
316 maximum frequency of the two jet species are typically separated by only a few degrees of  
317 latitude in the west Pacific. The west Pacific frequency maxima reaches its annual peak just east  
318 of Japan in January (Fig. 6c). This increased frequency appears related to an increased frequency  
319 of the subtropical jet. Despite a coherent increase in the polar jet frequency, the frequency of jet  
320 superpositions in the west Pacific decreases in February (Fig. 6d). In fact, despite the frequency  
321 and close proximity of the polar and subtropical jets during west Pacific winter, evident through  
322 a comparison of Figs. 4b-d and Figs. 5b-d, vertical superposition of the two species remains a  
323 rare event. Despite the annual maximum in Pacific basin polar jet frequency that characterizes  
324 March (Fig. 4e), the number of jet superpositions significantly decreases there in the same month  
325 (Fig. 6e). This decrease in frequency is likely tied to the corresponding decrease in the  
326 subtropical jet frequency (Fig. 4e).

327

### 328 *b. Additional characteristics of superposed jets*

329

330 In order to further characterize the nature of superposed jets, for each event identified in  
331 the 50-season climatology we examined the wind direction and speed at 250 hPa. The average  
332 250 hPa wind speed associated with all superpositions observed during November is  $77.0 \text{ m s}^{-1}$   
333 while the wind direction is solidly WSW (Fig. 7a). December has nearly as many WSW as W jet  
334 superpositions which are accompanied by an increase in the average wind speed to  $83.5 \text{ m s}^{-1}$   
335 (Fig. 7b). The primary wind direction for January jet superpositions veers back to westerly as  
336 over half of the superpositions in January are associated with a west wind (Fig. 7c). The average

337 wind speed also continues to increase reaching  $90.1 \text{ m s}^{-1}$  by this time. These observations make  
338 clear that superposed jets are some of the strongest jets found in the hemisphere. The speed and  
339 direction characteristics of February are nearly identical to January's with over half of  
340 superpositions associated with a westerly wind, while the average wind speed increases  
341 fractionally to  $90.3 \text{ m s}^{-1}$  (Fig. 7d). As spring approaches in the Northern Hemisphere the  
342 average wind speed of jet superpositions decreases to  $83.0 \text{ m s}^{-1}$  in March (Fig. 7e). The wind  
343 direction also begins to back as WSW is, once again, established as the most frequent wind  
344 direction.

345

#### 346 *c. Comparison to NDJFM mean zonal wind*

347

348 The Northern Hemisphere tropopause-level flow is often considered from the perspective  
349 of the zonal mean wind at some upper tropospheric isobaric level. Though this perspective is  
350 analytically simple, it fails to account for the more complicated distribution of the polar and  
351 subtropical jets revealed by the preceding analysis. Figure 8 illustrates aspects of the obfuscation  
352 engendered by this popular approach. The wintertime polar jet frequency maxima lie on the  
353 poleward edge of the 250 hPa seasonal mean zonal wind around the entire Hemisphere (Fig. 8a).  
354 In addition, the portions of the eastern Pacific and North Atlantic where the 250 hPa zonal mean  
355 wind fails to reach  $30 \text{ m s}^{-1}$  and yet the polar jet is found with regularity, suggests that the polar  
356 jet is highly variable in those regions. The subtropical jet frequency maxima, on the other hand,  
357 are found in the core of the average zonal wind isotachs from North Africa eastward to the  
358 central Pacific (Fig. 8b) suggesting a prominent role for the subtropical jet in the annual  
359 tropopause-level wind climatology over this vast area. Over North America, however, the  
360 subtropical jet is found on the equatorward edge of the average 250 hPa zonal wind, suggesting



361 that the average zonal wind in this region is nearly equally composed of polar jet and subtropical  
362 jet components. The jet superposition frequency maximum in the Pacific is displaced eastward  
363 and slightly poleward of the zonal wind maximum there. Whether this distribution suggests that  
364 superposition events in the west Pacific preferentially result from equatorward excursions of the  
365 polar jet at the entrance to the Pacific storm track is a subject for future inquiry. Similarly  
366 intriguing is the fact that the superposition maximum in the Atlantic is nearly coincident with the  
367 local zonal wind maximum (Fig. 8c).

368

## 369 **5. Summary and Discussion**

370

371 Jet streams or jets, defined as narrow, rapidly flowing currents of air located near the  
372 tropopause, often play a significant role in sensible weather in the mid-latitudes. Two species of  
373 jets have been identified in prior studies, the polar (or eddy-driven) jet and the subtropical jet.  
374 Some of the most significant findings regarding the large scale distribution of Northern  
375 Hemisphere jet streams were advanced by DT57, when they first published horizontal maps of  
376 tropopause heights. Since its introduction in 1957, the only amendment to DT57's conception of  
377 a three step tropopause structure came from Shapiro et al. (1987), who suggested the addition of  
378 the arctic jet and arctic tropopause step.

379 Though somewhat infrequently, the polar and subtropical jets occasionally become  
380 vertically superposed. Aside from scattered mentions in studies by Mohri (1953), Riehl (1962),  
381 Reiter (1961, 1963) and Reiter and Whitney (1969), such phenomena have only recently enjoyed  
382 renewed consideration (e.g. Winters and Martin 2014, 2016a,b and Handlos and Martin 2016).  
383 Motivated by the connections between jet superposition, significant weather events and large-  
384 scale circulation phenomena such as the EAWM, the present study has employed an objective

385 jetstream identification scheme to construct a 50-year cold season climatology of Northern  
386 Hemisphere polar, subtropical and superposed jets. The analysis demonstrates that cold season  
387 jet superposition events occur most often in the west Pacific near Japan, with other regional  
388 maxima residing over the southern U.S./North Atlantic and North Africa (Fig. 3c).  
389 Superposition events occur most (less) often during DJF (NM). In the west Pacific (North  
390 Atlantic), a maximum in the frequency of occurrence of the subtropical (polar) jet exists on  
391 average during the cold season. It is important to note that, despite the regional maximum in  
392 superposition frequency along with the close proximity of the polar (Fig. 4) and subtropical jets  
393 (Fig. 5) in the west Pacific, *jet superpositions are still relatively rare occurrences.*

394 In their examination of the distribution of Northern Hemisphere jet streams, Koch et al.  
395 (2006) used an integrated wind speed threshold to identify the jet streams. They further  
396 subdivided their jet identification into two subcategories; those jet features with shallow  
397 baroclinicity were classified as subtropical jets while those with deep baroclinicity were  
398 classified as polar jets. Broadly speaking, the results of their shallow baroclinicity classification  
399 correlate well with the findings presented in our work (their Fig. 6 compared to our Fig. 3b).  
400 When the deep baroclinicity classification is compared however, significant differences exist  
401 (their Fig. 7 and our Fig. 3a). First, their winter maximum in the deep baroclinicity (polar) jet in  
402 the Atlantic is less expansive than the Atlantic polar jet frequency maximum reported in the  
403 present analysis. Second, the Pacific basin is significantly different, with two maxima present in  
404 the Koch et al. analysis while, a single latitude band maxima is present in our analysis (Fig. 3a).  
405 Unfortunately, the Koch et al. (2006) classification scheme is not amenable to the identification  
406 of jet superposition events. The identification scheme introduced in this paper, which takes into  
407 account an integrated wind speed as well as a PV gradient threshold within specified tropopause-

408 crossing isentropic layers, allows each jet type to be identified separately and so also allows  
409 identification of jet superpositions.

410         The idealized modeling results of Lee and Kim (2003) suggested that a strong and  
411 poleward directed subtropical jet coincides with a more equatorward polar (eddy-driven) jet  
412 while a weaker, more zonal subtropical jet tends to be accompanied by increased poleward  
413 displacement of the polar jet. They further suggested that the west Pacific sector corresponds to  
414 a strong STJ regime while the Atlantic sector most often displays a weak STJ. Given the above  
415 associations, it is perhaps unsurprising that the frequency maxima of jet superpositions revealed  
416 by the present analysis occurs in the west Pacific basin (Fig. 3b).

417         The analysis and methodology presented in this paper provide a framework for objective  
418 identification of the tropopause-level polar and subtropical jets. Identification of the polar jet  
419 using near-surface or lower tropospheric winds is a popular approach (e.g. Lorenz and Hartmann  
420 2003, Hartmann 2007, Woollings et al. 2010, Barnes and Polvani 2013) that is consistent with its  
421 mid-latitude, eddy-driven origins. Despite the physical insights garnered by such studies, the  
422 eddy-driven jet perspective perhaps deemphasizes consideration of the tropopause break  
423 identified by DT57 as a characteristic of the polar jet. Geostrophic cold air advection along the  
424 polar jet axis often results in differential tilting across that tropopause break and a downward  
425 extrusion of stratospheric PV into the upper troposphere above 700 hPa (Shapiro 1981, Keyser  
426 and Pecnick 1985, Martin 2014), leading to the production of mid-tropospheric features that are  
427 ultimately responsible for the development of surface cyclones. Interest in such important  
428 structural and dynamical characteristics of polar jet life cycles motivates the alternative  
429 tropopause-based identification approach presented here.

430 Winters and Martin (2016a) examined the synoptic and mesoscale processes supporting  
431 jet superposition in two contrasting cases over the eastern United States. They found that  
432 ageostrophic transverse circulations associated with the jet circulations themselves were  
433 instrumental in producing a downward protrusion of high PV air between the two originally  
434 separate jet cores. In combination with latent heat release and irrotational flow associated with  
435 convection, this subsidence contributed to the production of the steep tropopause wall  
436 characteristic of the superposed jet environment. A novel isentropic partitioning of the  
437 perturbation PV was employed by Winters and Martin (2016b) to perform a piecewise PV  
438 inversion of the tropopause disturbances associated with the separate polar and subtropical jets.  
439 They found that the 3D circulation associated with the polar jet PV (the non-divergent wind  
440 associated with the subtropical jet PV) controlled the vertical (horizontal) restructuring of the  
441 tropopause associated with building the steep tropopause PV wall that attended the jet  
442 superposition in their case.

443 The work presented in this study motivates a number of additional research questions.  
444 One such question regards the frequency distributions of the polar, subtropical, and superposed  
445 jets in the Southern Hemisphere. Additionally, application of the Winters and Martin (2016b)  
446 analysis tools to selected cases in the west Pacific region is currently underway. Given that the  
447 polar and subtropical jets are frequently in very close proximity to one another there during the  
448 winter (as first suggested by Riehl (1962)), we hope to better understand why vertical  
449 superposition there is nonetheless so rare.

450 Additional future work, with implications for understanding changes in the general  
451 circulation in a warmer climate, will apply our identification scheme to the output from selected  
452 CMIP5 simulations. As the evidence for Arctic amplification increases and the pole-to-equator

453 temperature gradient relaxes in the lower troposphere, it is plausible that a warmer planet will be  
454 characterized by a hemispheric reduction of the polar jet. However, given the moist neutrality of  
455 the tropical atmosphere, any warming of the surface will be reflected by larger warming aloft.  
456 Therefore it is not inconceivable that a warmer planet will feature enhanced baroclinicity in the  
457 tropical/subtropical upper troposphere – lower stratosphere (UTLS), thus supporting a stronger  
458 subtropical jet.

459 Finally, the interaction between, and superposition of, the polar and subtropical jets –  
460 which has served as the focus of this paper – represents perhaps one of the most conspicuous and  
461 synoptic-scale manifestations of tropical/extratropical interaction. To the extent that the  
462 frequency and distribution of these features, along with the synoptic and mesoscale dynamics  
463 associated with them, are better understood, so will be the diagnoses and prognoses of weather  
464 systems in both the current and future climate.

465  
466 ACKNOWLEDGEMENTS: This work was funded by the National Science Foundation through  
467 grant AGS-1265182.

468

469

470

471

472

473

474

475

476

477

478

479

480

REFERENCES

- 480  
481  
482 Athanasiadis, P. J., J. M. Wallace, and J. J. Wettstein, 2010: Patterns of wintertime jet stream  
483 variability and their relation to the storm tracks. *J. Atmos. Sci.*, **67**, 1361–1381.  
484  
485 Barnes, E. A., L. Polvani, 2013: Response of the midlatitude jets, and of their variability, to  
486 increased greenhouse gases in the CMIP5 models. *J. Climate*, **26**, 7117–7135.  
487  
488 Bosart, L. F., G. J. Hakim, K. R. Tyle, M. A. Bedrick, W. E. Bracken, M. J. Dickinson,  
489 and D. M. Schultz, 1996: Large-scale antecedent conditions associated with the  
490 12-14 March 1993 cyclone (“Superstorm ’93”) over eastern North America. *Mon.*  
491 *Wea. Rev.*, **124**, 1865-1891.  
492  
493 Christenson, C. E., and J. E. Martin, 2012: The large-scale environment associated with the 25-  
494 28 April 2011 severe weather outbreak. In 16<sup>th</sup> Annual Severe Storms and Doppler Radar  
495 Conference, 31 March 2012. Des Moines, IA, National Weather Association: Norman,  
496 OK.  
497  
498 Defant, F., 1959: On hydrodynamic instability caused by an approach of subtropical and  
499 polarfront jet stream in northern latitudes before the onset of strong cyclogenesis. *The*  
500 *Atmosphere and Sea in Motion*, Ed. Bert Bolin, Rockefeller Institute Press, New York,  
501 NY., 305-325.  
502

503 \_\_\_\_\_, and H. Taba, 1957: The threefold structure of the atmosphere and the characteristics of  
504 the tropopause. *Tellus*, **9**, 259-275.

505

506 desJardins, M. L., K. F. Brill, and S. S. Schotz, 1991: Use of GEMPAK on UNIX workstations.  
507 *7<sup>th</sup> Int. conf. on Interactive Information and Processing Systems for Meteorology,*  
508 *Oceanography, and Hydrology*, New Orleans, LA, Amer. Meteor. Soc., 449-453.

509

510 Eichelberger, S. J., and D. L. Hartmann, 2007: Zonal jet structure and the leading mode of  
511 variability. *J. Climate*, **20**, 5149–5163.

512

513 Ertel, 1942b: Ein neuer hydrodynamischer Wirbelsatz. *Meteor. Z.*, **59**, 277–281.

514

515 Griffin, K. S., and J. E. Martin, 2016: Synoptic features associated with temporally coherent  
516 modes of variability of the north Pacific jet stream *J. Climate* , **29**, (submitted).

517

518 Handlos, Z. J., 2016: Composite and case study analyses of the large-scale environments  
519 associated with west Pacific polar and subtropical vertical jet superposition events. Ph.D.  
520 dissertation, Department of Atmospheric and Oceanic Sciences, University of Wisconsin  
521 – Madison, 168 pp.

522

523 \_\_\_\_\_, and J. E. Martin, 2016: Composite analysis of large-scale environments conducive to  
524 west Pacific polar/subtropical jet superposition *J. Climate* , **29**, (in press).

525

526 Hakim, G. J., D. Keyser, and L. F. Bosart, 1996: The Ohio Valley wave merger cyclogenesis  
527 event of 25-26 January 1978. Part II: Diagnosis using quasigeostrophic potential vorticity  
528 inversion. *Mon. Wea. Rev.*, **124**, 2176-2205.

529

530 Hartmann, D.L., 2007: The General Circulation of the Atmosphere and its  
531 Variability. *J. Meteor. Soc. Japan*, **85B**, 123-143.

532

533 Held, I. M., 1975: Momentum transport by quasi-geostrophic eddies. *J. Atmos. Sci.*, **32**, 1494-  
534 1497.

535

536 Hoskins, B. J., and P. Berrisford, 1988: A potential vorticity perspective of the storm of 15-16  
537 October 1987. *Weather*, **43**, 122-129.

538

539 Jaffe, S. C., J. E. Martin, D. J. Vimont, and D. J. Lorenz, 2011: A synoptic-climatology of  
540 episodic, sub-seasonal retractions of the Pacific jet. *J. Climate*, **24**, 2846-2860.

541

542 Kalnay et al., The NCEP/NCAR 40-year reanalysis project, *Bull. Amer. Meteor. Soc.*, **77**,  
543 437-470, 1996.

544

545 Kistler, Robert, and Coauthors, 2001: The NCEP–NCAR 50–year reanalysis: monthly means  
546 CD–ROM and documentation. *Bull. Amer. Meteor. Soc.*, **82**, 247–267.

547



548 Keyser, D., M. J. Pecnick, 1985: A two-dimensional primitive equation model of frontogenesis  
549 forced by confluence and horizontal shear. *J. Atmos. Sci.*, **42**, 1259–1282.  
550

551 \_\_\_\_\_, D. and M. A. Shapiro, 1986: A review of the structure and dynamics of upper-level  
552 frontal zones. *Mon. Wea. Rev.*, 114, 452-499.  
553

554

555 Knupp, K. R. et al., 2014: Meteorological overview of the devastating 27 April 2011 tornado  
556 outbreak. *Bull. Amer. Meteor. Soc.*, **95**, 1041–1062  
557

558 Koch, P., H. Wernli, and H. C. Davies, 2006: An event-based jet-stream climatology and  
559 typology. *Int. J. Climatol.*, **26**, 283-301.  
560

561 Koteswaram, P. 1953: An analysis of the high tropospheric wind circulation over India in  
562 winter. *Indian J. Meteor. Geophys.*, **4**, 13-21.  
563

564 \_\_\_\_\_, and S. Parthasarathy, 1954: The mean jet stream over India in the pre-monsoon and  
565 post-monsoon seasons and vertical motions associated with subtropical jet streams.  
566 *Indian J. Meteor. Geophys.*, **5**, 138-156.  
567

568 Krishnamurti, T. N., 1961: The subtropical jet stream of winter. *J. Meteor.*, **18**, 172-191.  
569

570 Lee, S., and H.-K. Kim, 2003: The dynamical relationship between subtropical and eddy-driven  
571 jets. *J. Atmos. Sci.*, **60**, 1490–1503.

572

573 Loewe, F., and V. Radok, 1950: A meridional aerological cross section in the Southwest  
574 Pacific. *J. Meteor.*, **7**, 58-65. (Revised 305-306).

575

576 Lorenz, D. J., and D. L. Hartmann, 2003: Eddy–zonal flow feedback in the Northern Hemisphere  
577 winter. *J. Climate*, **16**, 1212–1227.

578

579 Martin, J. E., 2014: Quasi-geostrophic diagnosis of the influence of vorticity advection on the  
580 development of upper level jet-front systems. *Quart. J. Roy. Meteor. Soc.*, **140**, 2658-  
581 2671.

582

583 McWilliams, J. C., and J. H. S. Chow, 1981: Equilibrium geostrophic turbulence I: Reference  
584 solution in a  $\beta$ -plane channel. *J. Phys. Oceanogr.*, **11**, 921-949.

585

586 Mecikalski, J. R., and G. J. Tripoli, 1998: Inertial available kinetic energy and the dynamics of  
587 tropical plume formation. *Mon. Wea. Rev.*, **126**, 2200-2216.

588

589 Mohri, K., 1953: On the fields of wind and temperature over Japan and adjacent waters during  
590 winter of 1950-1951. *Tellus*, **5**, 340-358.

591

592 Morgan, M. C., and J. W. Nielsen-Gammon, 1998: Using tropopause maps to diagnose  
593 midlatitude weather systems. *Mon. Wea. Rev.*, **126**, 2555-2579.

594

595 Namias, J., and P. F. Clapp, 1949: Confluence theory of the high tropospheric jet  
596 stream. *J. Meteor.*, **6**, 330–336.

597

598 Newton, C. W., 1954: Frontogenesis and frontolysis as a three-dimensional process. *J.*  
599 *Meteor.*, **11**, 449-461.

600

601 Palmén, E., and C. W. Newton, 1969: *Atmospheric Circulation Systems: Their Structure and*  
602 *Physical Interpretation*. Academic Press, 603 pp.

603

604 Panetta, R. L., 1993: Zonal jets in wide baroclinically unstable regions: Persistence and scale  
605 selection. *J. Atmos. Sci.*, **50**, 2073-2106.

606

607 Randel, W. J., D. J. Seidel, and L. L. Pan, 2007: Observational characteristics of double  
608 tropopauses. *J. Geophys. Res.*, **112**, D07309, doi:10.1029/2006JD007904.

609

610 Reiter, E. R., 1961: *Meteorologie der Strahlströme (Meteorology of the Jet Streams)*. Springer-  
611 Verlag, Vienna, 473 pp.

612

613 Reiter, E. R., 1963: *Jet Stream Meteorology*. University of Chicago Press, 515 pp.

614

615 \_\_\_\_\_, and L. F. Whitney, 1969: Interaction between subtropical and polar-front jet stream. *Mon.*  
616 *Wea. Rev.*, **97**, 432–438. doi: <http://dx.doi.org/10.1175/1520->  
617 [0493\(1969\)097<0432:IBSAPJ>2.3.CO;2](http://dx.doi.org/10.1175/1520-0493(1969)097<0432:IBSAPJ>2.3.CO;2).

618

619 Riehl, H., 1962: Jet streams of the atmosphere, *Technical Report No. 32*. Department of  
620 Atmospheric Science, Colorado State University, Fort Collins, CO, 117.

621

622 Rhines, P. B., 1975: Waves and turbulence on a  $\beta$ -plane. *J. Fluid. Mech.*, **69**, 417-433.

623

624 Shapiro, M. A., 1981: Frontogenesis and geostrophically forced secondary circulations in the  
625 vicinity of jet stream-frontal zone systems. *J. Atmos. Sci.*, **38**, 954-973.

626

627 \_\_\_\_\_, 1985: Dropwindsonde observations of an Icelandic Low and a Greenland mountain-lee  
628 wave. *Mon. Wea. Rev.*, **113**, 680-683.

629

630 \_\_\_\_\_, M. A., Oltmans, S.J., Bodhaine, B.A. and Schnell, R.C. (1984). El Chichón volcanic  
631 debris in an Arctic tropopause fold. *Geophysical Research Letters* 11:  
632 [doi:10.1029/0GPRLA000011000005000421000001](https://doi.org/10.1029/0GPRLA000011000005000421000001).

633

634 \_\_\_\_\_, T. Hampel, and A. J. Krueger, 1987: The Arctic tropopause fold. *Mon. Wea.Rev.*, **115**,  
635 444-454.

636

637 \_\_\_\_\_, and D. Keyser, 1990: Fronts, jet streams and the tropopause. *Extratropical*  
638 *Cyclones: The Erik Palmen Memorial Volume*, C. Newton and E. O. Holopainen, Eds.,  
639 Amer. Meteor. Soc., 167-191.

640

641 \_\_\_\_\_, H. Wernli, J. Bao, J. Methven, X. Zou, J. Doyle, T. Holt, E. Donall-Grell, and P.  
642 Neiman, 1999: A planetary-scale to mesoscale perspective of the life cycles of  
643 extratropical cyclones: The bridge between theory and observations. *The Life Cycle of*  
644 *Extratropical Cyclones*, Eds. M. A. Shapiro and S. Gronas, Amer. Meteor. Soc.,  
645 139-185.

646

647 Sutcliffe, R. C., and J. K. Bannon, 1954: *Seasonal changes in the upper-air conditions in the*  
648 *Mediterranean Middle East area*. Sci. Proc. International Assoc. Meteor. (UGGI), Rome  
649 1954.

650

651 \_\_\_\_\_, and \_\_\_\_\_, 2014: The role of a polar/subtropical jet superposition in the May 2010  
652 Nashville Flood. *Wea. Forecasting*,**29**, 954-974.

653

654 \_\_\_\_\_, and \_\_\_\_\_, 2016a: Synoptic and mesoscale processes supporting vertical superposition of  
655 the polar and subtropical jets in two contrasting cases *Quart. J. Roy. Meteor. Soc.*,**142**,  
656 1133-1149.

657

658 \_\_\_\_\_, and \_\_\_\_\_, 2016b: Diagnosis of a North American polar/subtropical jet superposition  
659 employing potential vorticity inversion. *Mon. Wea. Rev.*,**144**, (submitted).

660

661 Woollings, T., A. Hannachi and B. Hoskins, 2010: Variability of the North Atlantic eddy-driven  
662 jet stream, Q. J. R. Meteorol. Soc., 649, 856-868.

663

664 Yeh, T. C., 1950: The circulation of the high troposphere over China in the winter of 1945-46.  
665 *Tellus*, **2**, 173-183.

666

667

667

668

## LIST OF FIGURES

669 **Figure 1:** (a) 300 hPa isotachs (shaded every  $10 \text{ m s}^{-1}$  starting at  $30 \text{ m s}^{-1}$ ) at 0000 UTC 27 April  
670 2010 depicting separate polar and subtropical jets. (b) Cross section along A-A' in Fig. 1a. Solid  
671 black (blue) lines are isertels of 1, 2, 3 (4-9) PVU ( $1 \text{ PVU} = 10^{-6} \text{ K m}^2 \text{ kg}^{-1} \text{ s}^{-1}$ ). Dashed lines are  
672 isentropes contoured every 5K. Red solid lines are isotachs labeled in  $\text{m s}^{-1}$  and contoured every  
673  $10 \text{ m s}^{-1}$  starting at  $30 \text{ m s}^{-1}$ . The jet cores are shaded yellow and the 315:330K and 340:355K  
674 isentropic layers are shaded gray. The blue (red) line corresponds to a grid column in which the  
675 black dot confirms a polar (subtropical) jet identification. (c) As in (a) but at 0000 UTC 24  
676 October 2010. (d) As in (b) but along the cross section B-B' in Fig. 1c. The blue line  
677 corresponds to a grid column in which a jet superposition (i.e. a polar and subtropical jet in the  
678 same column) is identified.

679

680 **Figure 2:** (a) Cold season average of zonally averaged  $\Delta y$  (km) for 5K isentropic layers ranging  
681 from 300-305K to 365-370K. The 315-330K and 340-355K layers are highlighted in light gray  
682 shading. (b) The average frequency of occurrence of grid points with a maximum wind speed  
683 value within the 5K isentropic layers along the abscissa per cold season. The 315-330K and  
684 340-355K layers are shaded in blue and red, respectively.

685

686 **Figure 3:** Cold season average frequency of occurrence of Northern Hemisphere (a) polar jet, (b)  
687 subtropical jet, and (c) superposed jet ID's for the 1960/61 – 2009/10 seasons.

688

689 **Figure 4:** Monthly average frequency of occurrence of Northern Hemisphere polar jet ID's for  
690 the month of a) November, b) December, c) January, d) February and e) March.

691

692 **Figure 5:** Same as Fig. 4 but for Northern Hemisphere subtropical jet ID's.

693

694 **Figure 5 (continued):** (g) As in Fig. 5a but for March. (h) As in Fig. 5a but for April. (i) As in  
695 Fig. 5a but for May. (j) As in Fig. 5a but for June. (k) As in Fig. 5a but for July. (l) As in Fig. 5a  
696 but for August.

697

698 **Figure 6:** Same as Fig. 4 but for Northern Hemisphere superposed jet ID's.

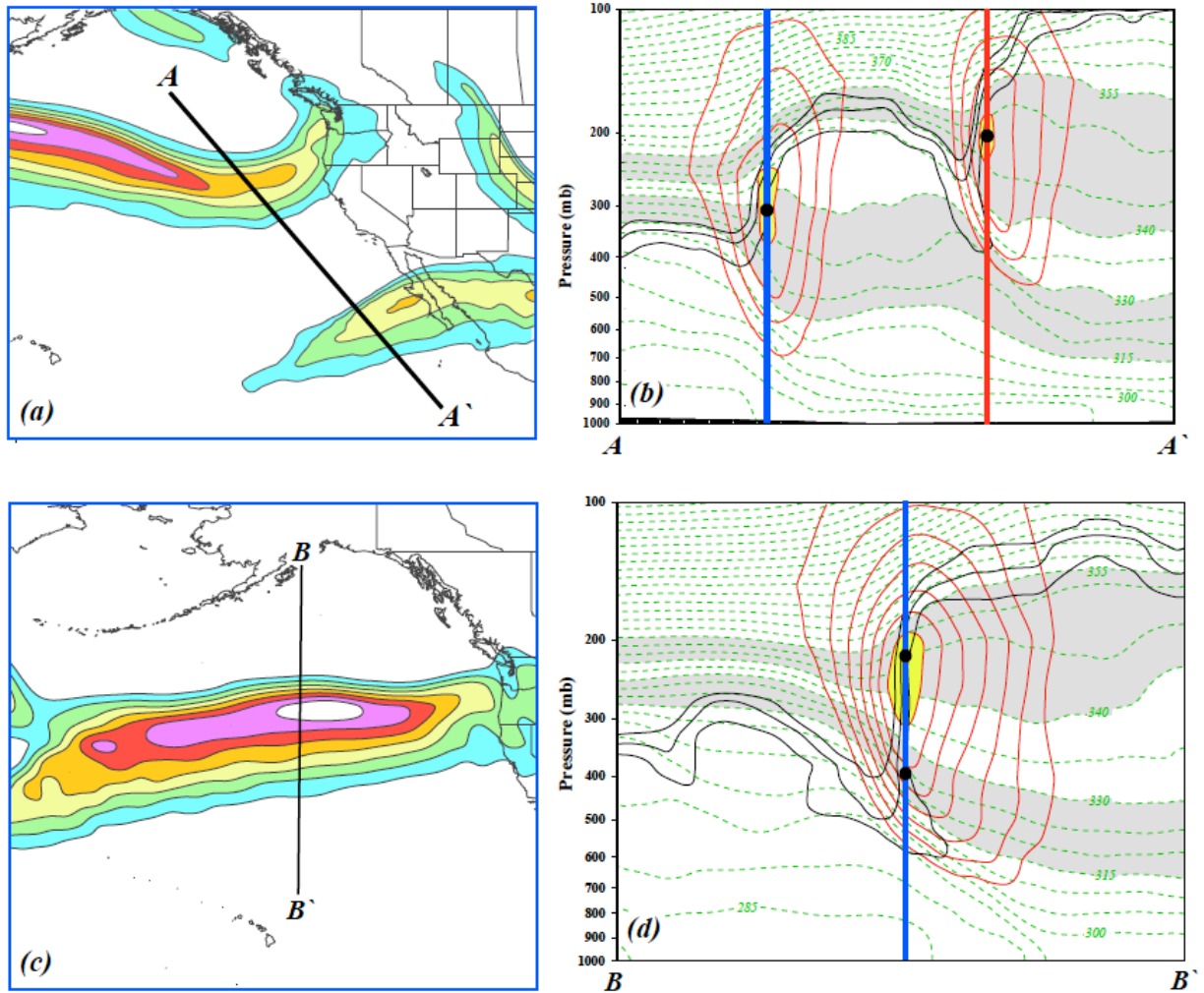
699

700 **Figure 7:** (a) Wind direction plotted on the wind rose for every Northern Hemisphere jet  
701 superposition identified during the month of September over the period 1960-2010. Average  
702 wind speed for each jet superposition in  $\text{m s}^{-1}$  shown in blue on bar graph. (b) As in Fig. 8a but  
703 for but for October. (c) As in Fig. 8a but for but for November. (d) As in Fig. 8a but for but for  
704 December.

705

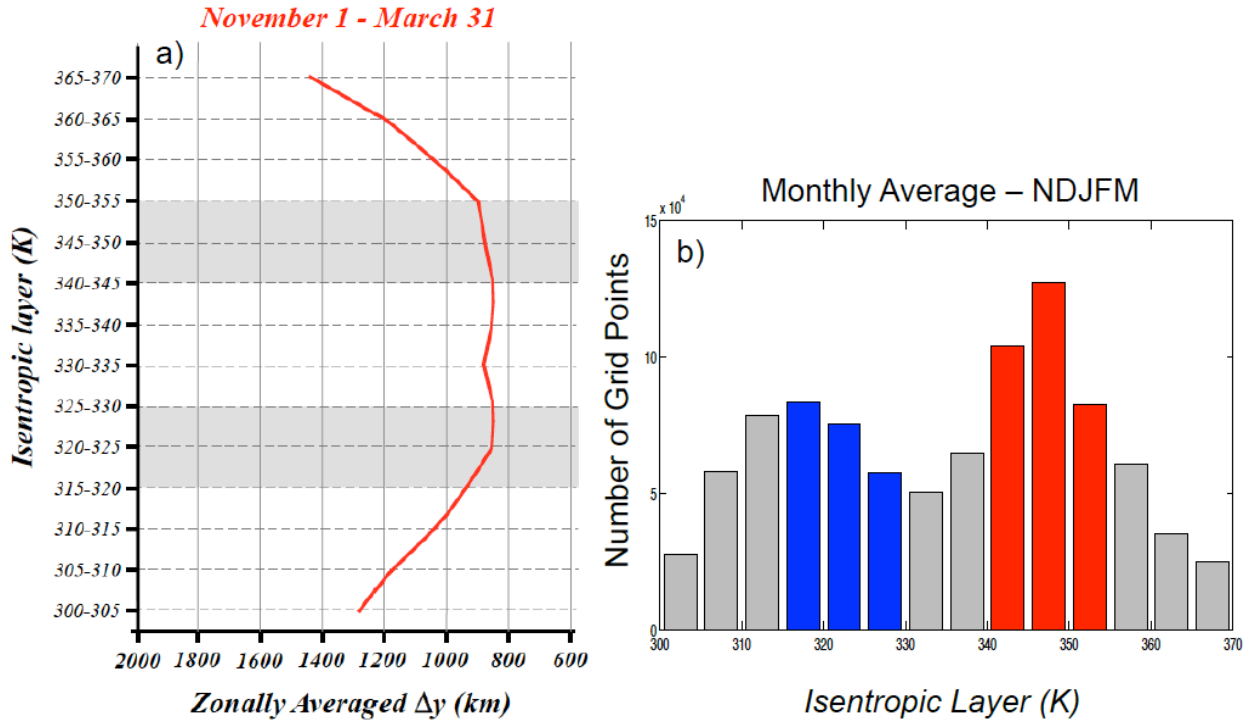
706 **Figure 8:** Same as Fig. 3 but with the cold season climatological 250 hPa zonal wind plotted  
707 every  $10 \text{ m s}^{-1}$  starting at  $30 \text{ m s}^{-1}$  in thick, black solid contour.





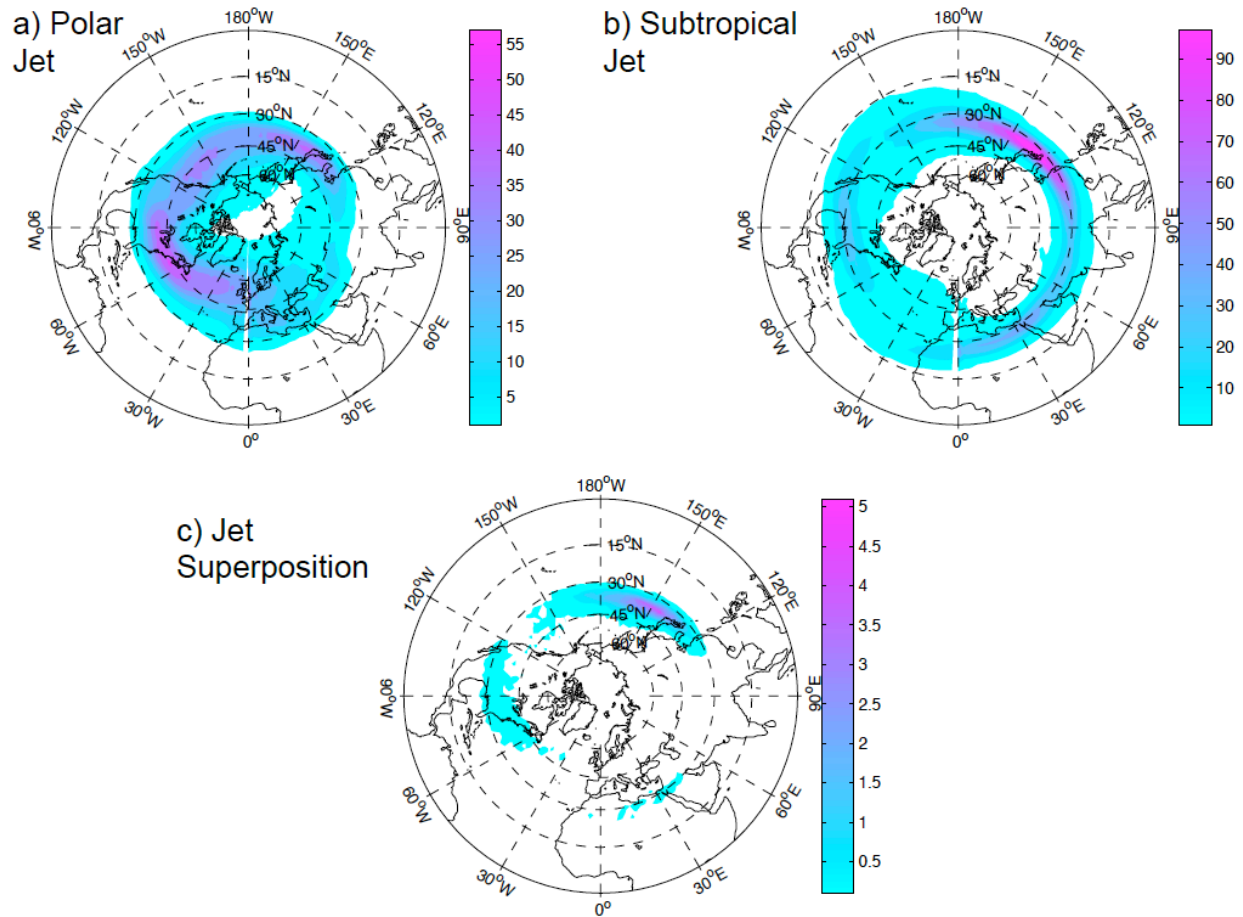
708

709 **Figure 1:** (a) 300 hPa isotachs (shaded every  $10 \text{ m s}^{-1}$  starting at  $30 \text{ m s}^{-1}$ ) at 0000 UTC 27 April  
 710 2010 depicting separate polar and subtropical jets. (b) Cross section along A-A' in Fig. 1a. Solid  
 711 black (blue) lines are isertels of 1, 2, 3 (4-9) PVU ( $1 \text{ PVU} = 10^{-6} \text{ K m}^2 \text{ kg}^{-1} \text{ s}^{-1}$ ). Dashed lines are  
 712 isentropes contoured every 5K. Red solid lines are isotachs labeled in  $\text{m s}^{-1}$  and contoured every  
 713  $10 \text{ m s}^{-1}$  starting at  $30 \text{ m s}^{-1}$ . The jet cores are shaded yellow and the 315:330K and 340:355K  
 714 isentropic layers are shaded gray. The blue (red) line corresponds to a grid column in which the  
 715 black dot confirms a polar (subtropical) jet identification. (c) As in (a) but at 0000 UTC 24  
 716 October 2010. (d) As in (b) but along the cross section B-B' in Fig. 1c. The blue line  
 717 corresponds to a grid column in which a jet superposition (i.e. a polar and subtropical jet in the  
 718 same column) is identified.  
 719



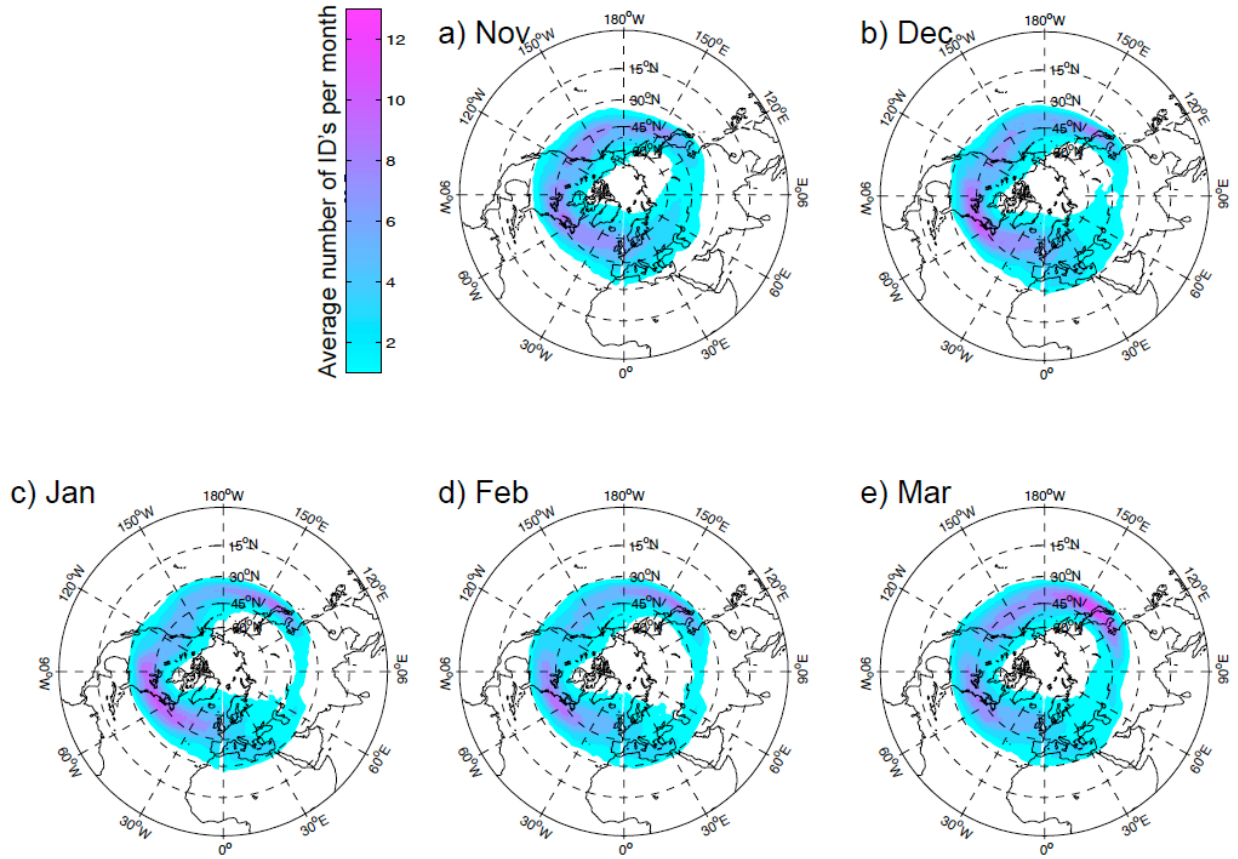
720

721 **Figure 2:** (a) Cold season average of zonally averaged  $\Delta y$  (km) for 5K isentropic layers ranging  
 722 from 300-305K to 365-370K. The 315-330K and 340-355K layers are highlighted in light gray  
 723 shading. (b) The average frequency of occurrence of grid points with a maximum wind speed  
 724 value within the 5K isentropic layers along the abscissa per cold season. The 315-330K and  
 725 340-355K layers are shaded in blue and red, respectively.



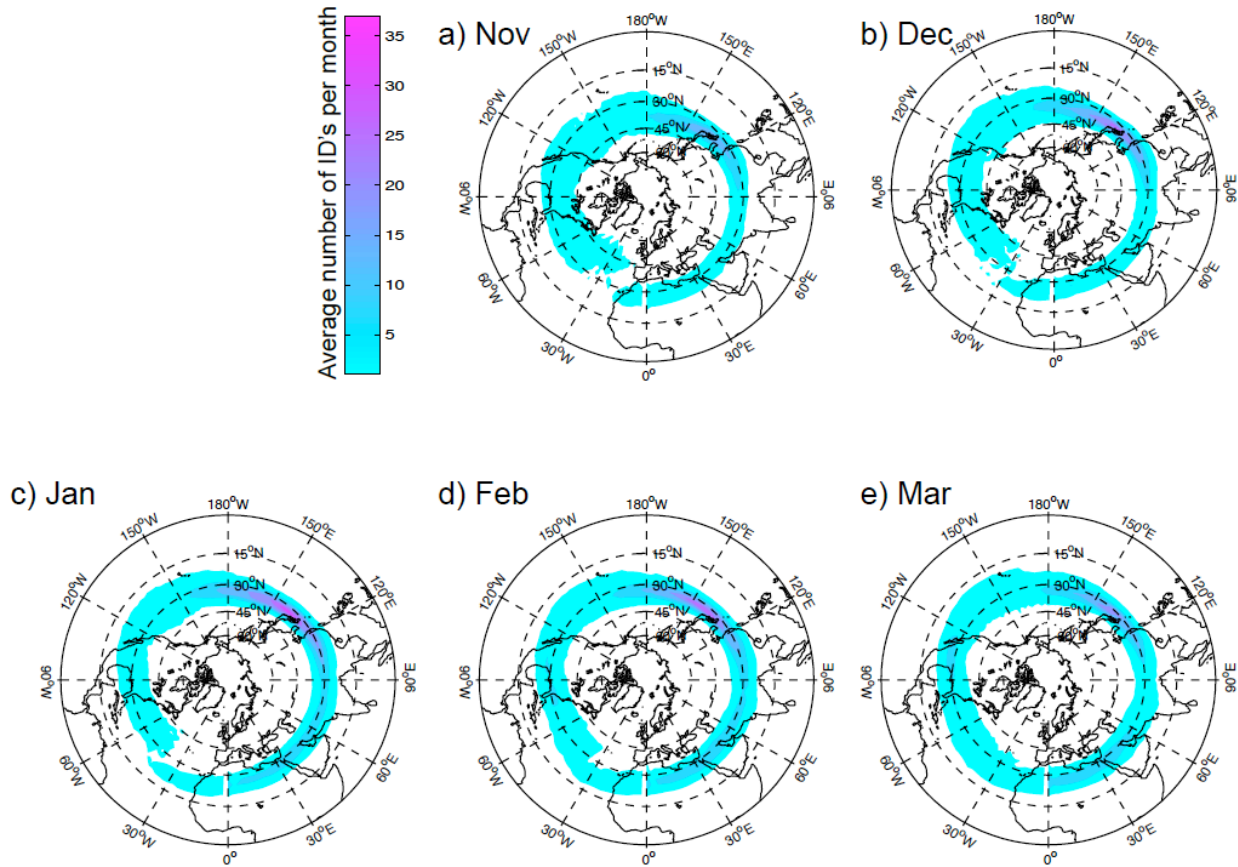
726

727 **Figure 3:** Cold season average frequency of occurrence of Northern Hemisphere (a) polar jet, (b)  
 728 subtropical jet, and (c) superposed jet ID's for the 1960/61 – 2009/10 seasons.



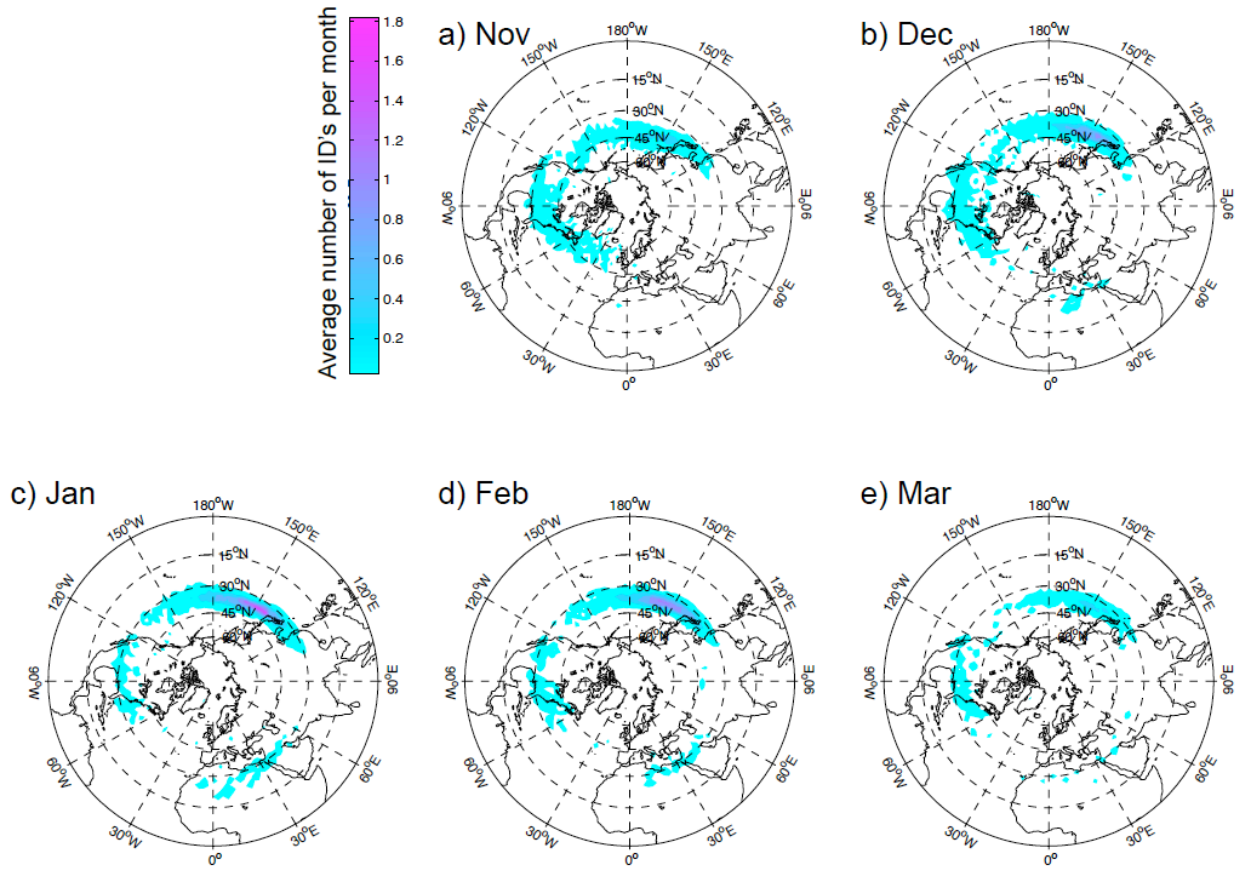
729  
730  
731

**Figure 4:** Monthly average frequency of occurrence of Northern Hemisphere polar jet ID's for the month of a) November, b) December, c) January, d) February and e) March.



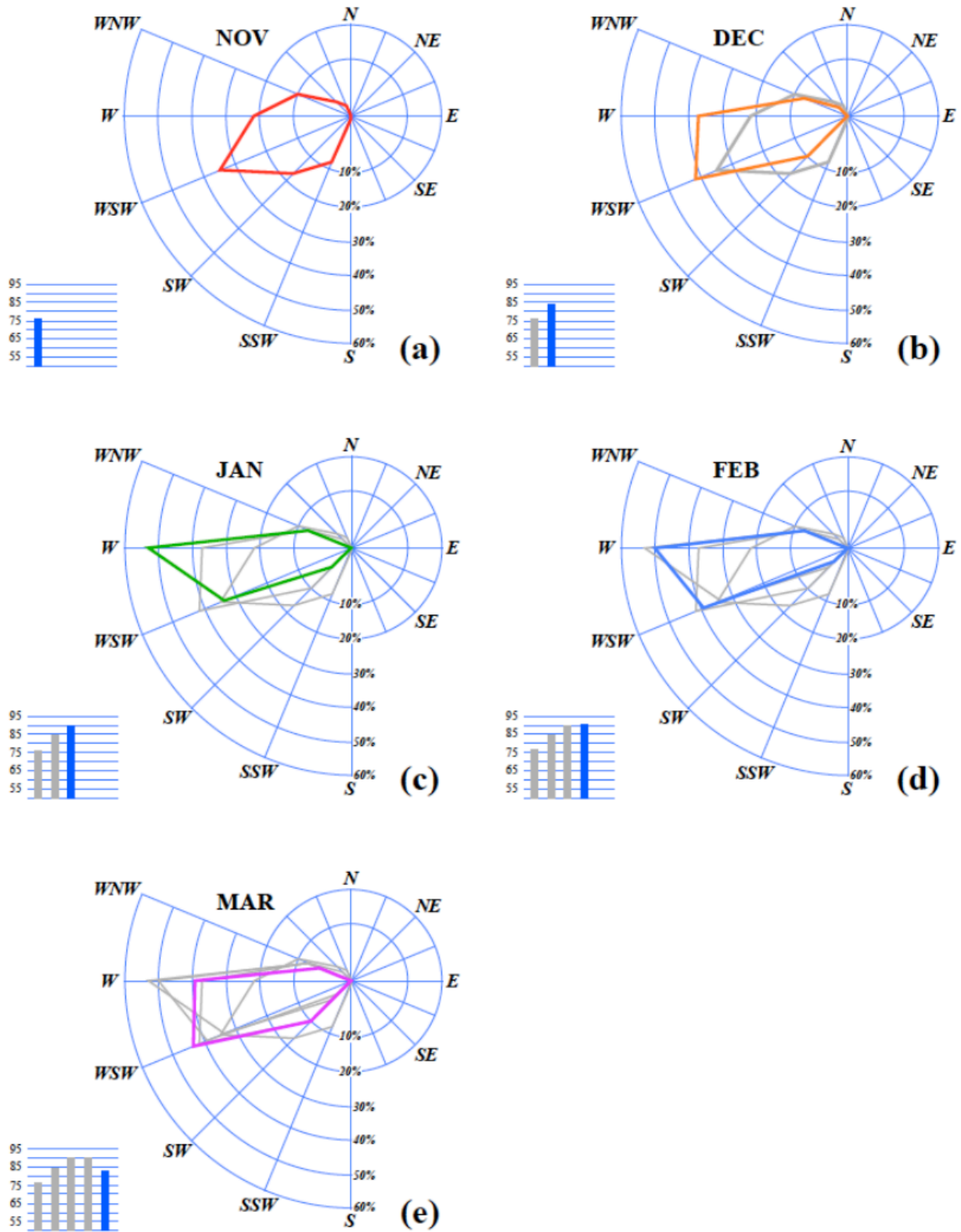
732  
733

**Figure 5:** Same as Fig. 4 but for Northern Hemisphere subtropical jet ID's.



734  
735  
736

**Figure 6:** Same as Fig. 4 but for Northern Hemisphere superposed jet ID's.

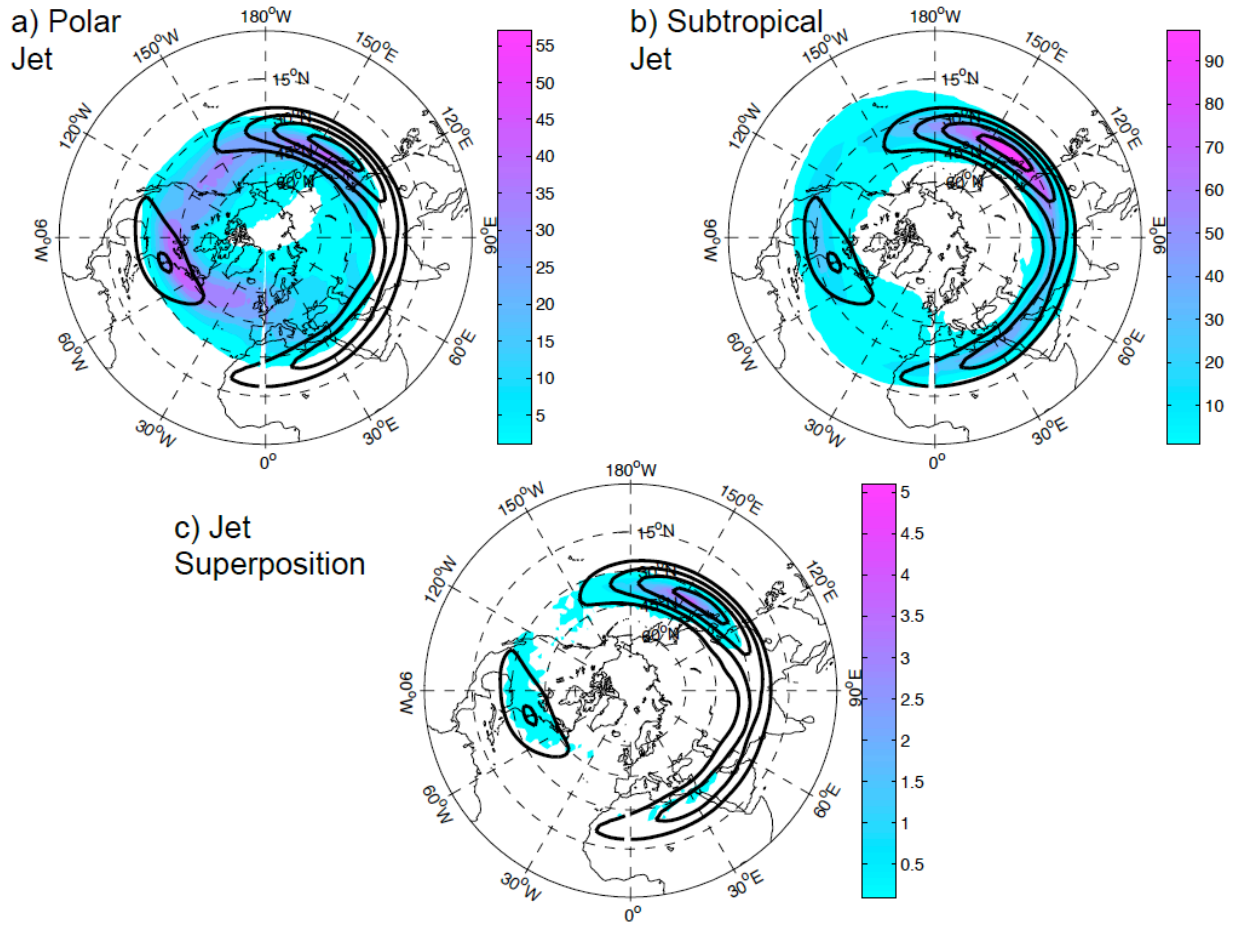


737  
 738 **Figure 7:** (a) Wind direction plotted on the wind rose for every Northern Hemisphere jet  
 739 superposition identified during the 50 Novembers in the analysis. Average wind speed for each

740 jet superposition in  $\text{m s}^{-1}$  shown in blue on bar graph. (b) As in Fig. 7a but for but for December.  
741 The thin gray line on the wind rose and gray bar graph represents prior month's direction and  
742 speed data. (c) As in Fig. 7b but for but for January. (d) As in Fig. 7b but for but for February.  
743 (e) As in Fig. 7b but for March.

744  
745  
746  
747  
748  
749  
750  
751  
752  
753  
754  
755  
756  
757  
758  
759  
760  
761





762  
 763 **Figure 8:** Same as Fig. 3 but with the cold season climatological 250 hPa zonal wind plotted  
 764 every 10 m s<sup>-1</sup> starting at 30 m s<sup>-1</sup> in thick, black solid contour.